

The Helicity Sign of Flux Transfer Event Flux Ropes and its Relationship to the Guide Field and Hall Physics in Magnetic Reconnection at the Magnetopause

S. Dahani¹, R. Kieokaew¹, V. Génot¹, B. Lavraud^{1,2}, Y. Chen³, B.
Michotte de Welle⁴, N. Aunai⁴, G. Tóth⁵, P. A. Cassak⁶, N. Fargette¹, R.
C. Fear⁷, A. Marchaudon¹, D. Gershman⁸, B. Giles⁸, R. Torbert⁹, J.
Burch¹⁰

¹Institut de Recherche en Astrophysique et Planétologie, CNRS, UPS, CNES, Université de Toulouse,
Toulouse, France

²Laboratoire d'Astrophysique de Bordeaux, Univ. Bordeaux, CNRS, Pessac, France

³Department of Astrophysical Sciences and Princeton Plasma Physics Laboratory, Princeton University,
Princeton, NJ 08540, USA

⁴Laboratory of Plasma Physics, CNRS, Ecole Polytechnique, UPMC, Université Paris Sud, Orsay, France

⁵Department of Climate and Space Sciences and Engineering, University of Michigan, Ann Arbor, MI,
USA

⁶Department of Physics and Astronomy and center for KINETIC Plasma Physics, West Virginia
University, Morgantown, WV, USA

⁷School of Physics & Astronomy, University of Southampton, Southampton, UK

⁸NASA Goddard Space Flight Center, Greenbelt, MD, USA

⁹Space Science Center, University of New Hampshire, Durham, NH, USA

¹⁰Southwest Research Institute, San Antonio, TX, USA

Key Points:

- We study the helicity sign of Flux Transfer Events and investigate upstream solar wind conditions and local magnetic shear around them.
- The helicity sign is found to be unassociated to the Interplanetary Magnetic Field (BY) component when the local magnetic shear is high.
- The FTEs' helicity sign in such cases may relate to the Hall field of magnetic reconnection in the absence of a guide field.

Corresponding author: Souhail Dahani, sdahani@irap.omp.eu

This is the author manuscript accepted for publication and has undergone full peer review but has not been through the copyediting, typesetting, pagination and proofreading process, which may lead to differences between this version and the [Version of Record](#). Please cite this article as [doi: 10.1029/2022JA030686](https://doi.org/10.1029/2022JA030686).

This article is protected by copyright. All rights reserved.

Abstract

Flux Transfer Events (FTEs) are transient magnetic flux ropes typically found at the Earth's magnetopause on the dayside. While it is known that FTEs are generated by magnetic reconnection, it remains unclear how the details of magnetic reconnection controls their properties. A recent study showed that the helicity sign of FTEs positively correlates with the east-west (B_y) component of the Interplanetary Magnetic Field (IMF). With data from the Cluster and Magnetospheric Multiscale missions, we performed a statistical study of 166 quasi force-free FTEs. We focus on their helicity sign and possible association with upstream solar wind conditions and local magnetic reconnection properties. Using both in situ data and magnetic shear modeling, we find that FTEs whose helicity sign corresponds to the IMF B_y are associated with moderate magnetic shears while those that do not correspond to the IMF B_y are associated with higher magnetic shears. While uncertainty in IMF propagation to the magnetopause may lead to randomness in the determination of the flux rope core field and helicity, we rather propose that for small IMF B_y , which corresponds to high shear and low guide field, the Hall pattern of magnetic reconnection determines the FTE core field and helicity sign. In that context we explain how the temporal sequence of multiple X-line formation and the reconnection rate are important in determining the flux rope helicity sign. This work highlights a fundamental connection between kinetic processes at work in magnetic reconnection and the macroscale structure of FTEs.

Plain Language Summary

In the vicinity of the Earth's magnetosphere outer boundary, the magnetopause, twisted magnetic field structures known as "Flux Transfer Events" (FTEs) are often detected by spacecraft in-situ. They temporarily connect the solar wind to the Earth's ionosphere, allowing the transfer of solar wind flux into the magnetosphere. It is known that FTEs are produced as a consequence of magnetic reconnection, a process that rearranges the topology of sheared magnetic fields, between the shocked solar wind and the geomagnetic field. However, our understanding of how the microphysics of magnetic reconnection can lead to the macroscopic structures of FTEs is still limited. We revisit the in-situ observations of FTEs made by the Cluster and Magnetospheric Multiscale missions. We focus on the twist feature of FTEs as characterized by their helicity and investigate its relationship to solar wind conditions and possible link to magnetic reconnection prop-

62 erties. By investigating local magnetic shear conditions around FTE locations, we found
63 that the FTE helicity is determined by a kinetic feature of magnetic reconnection known
64 as the “Hall magnetic field”. Our study highlights a close connection between a kinetic
65 process of magnetic reconnection and the global structure of FTEs, constituting a cross-
66 scale coupling effect in solar-terrestrial interaction.

67 1 Introduction

68 Flux Transfer Events (FTEs) are magnetic flux ropes produced at the dayside mag-
69 netopause as a consequence of magnetic reconnection. They were first observed by Russell
70 and Elphic (1978) using magnetic field measurement from ISEE 1 and 2. An FTE is recog-
71 nised in in-situ spacecraft time-series data as a bipolar variation in the magnetic field
72 component normal to the magnetopause (*i.e.*, magnetic field B_N). The bipolar signa-
73 ture consists of a variation of the magnetic field from positive to negative or negative to
74 positive as reported by Russell and Elphic (1979) and Rijnbeek et al. (1982). For typ-
75 ical FTEs, the bipolar signature is co-located with an enhancement in the magnetic field
76 strength compared to the ambient field (*e.g.*, Paschmann et al., 1982), although this en-
77 hancement may depend on the spacecraft trajectory (*e.g.*, H. Zhang et al., 2010). A less-
78 common type of FTEs, called crater FTEs (*e.g.*, LaBelle et al., 1987; Farrugia et al., 1988;
79 Sibeck et al., 2008; H. Zhang et al., 2010; Farrugia et al., 2011; Trenchi et al., 2019), has
80 dips at the center of the enhanced magnetic field strength; it was suggested to be a sig-
81 nature of early-stage FTEs (H. Zhang et al., 2010, 2012).

82 Various mechanisms were suggested to explain the formation of FTEs. Lee and Fu
83 (1985) proposed that an FTE is created between two reconnection X-lines formed simul-
84 taneously on the dayside magnetopause. Using global magnetohydrodynamics (MHD)
85 simulations, Raeder (2006) showed that FTEs can be generated by sequential, magnetic
86 reconnection where reconnection X-lines are formed one after the other under a large dipole
87 tilt condition (*e.g.*, during the winter/summer season on the Northern/Southern hemi-
88 sphere); Dorelli and Bhattacharjee (2009) later showed that the dipole tilt is not required
89 to produce FTEs. Other formation mechanisms were also proposed based on single X-
90 line reconnection due to the nature of unsteady or transient reconnection (*e.g.*, South-
91 wood et al., 1988; Scholer, 1988). More recently, there are increasing evidence support-
92 ing FTE generation due to multiple X-line reconnection (*e.g.*, Hasegawa et al., 2010; Øieroset
93 et al., 2011; Trenchi et al., 2011; Kieokaew et al., 2021). After their initial formation, FTEs

94 undergo dynamical evolution due to continuous reconnection while propagating poleward
 95 (*e.g.*, Akhavan-Tafti et al., 2019; Hoilijoki et al., 2019; Hwang et al., 2020; Guo et al.,
 96 2021). Using a 2-D hybrid-Vlasov simulation, Akhavan-Tafti et al. (2020) demonstrated
 97 that magnetic islands (magnetic flux ropes in 3-D) can coalesce, erode, or divide due to
 98 reconnection at their periphery during the evolution. Such dynamical processes were be-
 99 lieved to lead to FTE growth after their generation. In this study, we mainly focus on
 100 the FTE generation by the classical scenarios which involve single and multiple X-line
 101 reconnection.

102 An FTE flux rope has a helical, twisted interior (*e.g.*, Russell & Elphic, 1979; Cow-
 103 ley, 1982; Saunders et al., 1984). Magnetic helicity is an ideal MHD invariant defined as
 104 $\mathcal{H} = \int_V \mathbf{A} \cdot \mathbf{B} dV$, where \mathbf{A} is the magnetic vector potential, \mathbf{B} is the magnetic field,
 105 and V is the integration volume. Magnetic helicity is a useful quantity for characteriz-
 106 ing topology of magnetic structures (*e.g.*, Berger & Field, 1984; Song & Lysak, 1989; Berger,
 107 1999; Wright & Berger, 1990). In particular, the sign of magnetic helicity, namely “hand-
 108 edness”, or “chirality”, has been used to characterize the sense of the twist in the flux
 109 rope interior into right-handed ($H = +1$) and left-handed ($H = -1$) (*e.g.*, Burlaga,
 110 1988; Lepping et al., 1990; Bothmer & Schwenn, 1998). Studies of the helicity sign of
 111 magnetic flux ropes in various environments such as in interplanetary space (*e.g.*, Both-
 112 mer & Schwenn, 1998; Dasso et al., 2003; Leamon et al., 2004; Pal, 2022), planetary mag-
 113 netospheres (*e.g.*, Russell, 1990; Wei et al., 2010; Martin et al., 2020), and Earth’s mag-
 114 netosphere (*e.g.*, H. Zhang et al., 2010; Eastwood et al., 2012; Kieokaew et al., 2021) have
 115 led to a better understanding of their origins. The total magnetic helicity, defined in a
 116 volume bounded by perfectly conducting walls, is generally conserved. During magnetic
 117 reconnection, the total magnetic helicity remains conserved as well (*e.g.*, Berger, 1982,
 118 1984), on time scales shorter than the global diffusion time scale. In this study, we do
 119 not calculate the full helicity but merely focus on the sign of magnetic helicity as obtained
 120 from fitting magnetic field data to a constant-alpha force-free flux rope model (*e.g.*, Burlaga,
 121 1988; Lepping et al., 1990).

122 Recently, Kieokaew et al. (2021) studied the helicity sign of FTEs and its relation-
 123 ship with the Interplanetary Magnetic Field (IMF). They found that the helicity sign
 124 of most FTEs correlates to the IMF B_y polarity, further revealing a close relationship
 125 between solar wind conditions and the formation of FTEs. Based on geometrical con-
 126 siderations of FTE formation under southward IMF conditions, they hypothesised that

127 the flux rope twist direction should correspond to the IMF B_y orientation. This hypoth-
 128 esis arose from the configuration of magnetic reconnection in which the IMF B_y com-
 129 ponent would give a guide field to the reconnecting magnetic field between the draped,
 130 southward IMF and the northward geomagnetic field (Lee & Fu, 1985). In the context
 131 of FTE generation by multiple X-line reconnection, this guide field (IMF B_y) orienta-
 132 tion would directly determine the core field and the helicity sign of the flux rope formed
 133 between the two X-lines. Under southward IMF, an FTE formed in between multiple
 134 X-line reconnection would have a positive helicity sign if it is formed under IMF $B_y >$
 135 0 (*i.e.*, duskward), while it would have a negative helicity sign if it is formed under IMF
 136 $B_y < 0$ (*i.e.*, dawnward). Using data from the Magnetospheric MultiScale (MMS) mis-
 137 sion, they performed a statistical study of the helicity sign of FTE flux ropes. They found
 138 that the majority of events are consistent with this hypothesis. However, there were a
 139 significant number of events (14 out of 84) that were not consistent with this hypoth-
 140 esis; they called them the outliers, and we will keep this definition in the present work.
 141 In other words, in some events, a duskward IMF B_y imposed both a duskward core field
 142 and a positive helicity, and in others, a dawnward IMF B_y imposed both a dawnward
 143 core field and a negative helicity. Figure 1, adapted from Kieokaew et al. (2021), shows
 144 a schematic illustration of a dawnward and southward IMF leading to a dawnward core
 145 field and left-handed flux rope. A duskward and southward IMF would have led to a duskward
 146 core field and a right-handed flux rope, highlighting the one-to-one relationship between
 147 the core field orientation and the helicity sign that results from guide field reconnection
 148 in a scenario where the flux rope is formed by multiple X-lines. In another study, Karimabadi
 149 et al. (1999) discussed, based on 2-D and 3-D hybrid simulations, how the core field of
 150 flux ropes on the dayside magnetopause and the magnetotail are controlled by the guide
 151 field. Teh, Abdullah, and Hasbi (2014) studied the core field of two flux ropes observed
 152 at the magnetopause under high magnetic shear. They found that the polarity of the
 153 core field of one of the flux ropes is opposite to the guide field produced by reconnect-
 154 tion as observed near the flux ropes. In this work, we expand the statistics of Kieokaew
 155 et al. (2021) by including FTE observations from the Cluster mission. We investigate
 156 in particular the FTE population whose helicity sign is inconsistent with the IMF B_y
 157 orientation to understand their formation mechanism.

158 Here, we investigate the structures of FTEs using the sign of magnetic helicity as
 159 a tool to better understand their formation and connection to magnetic reconnection.

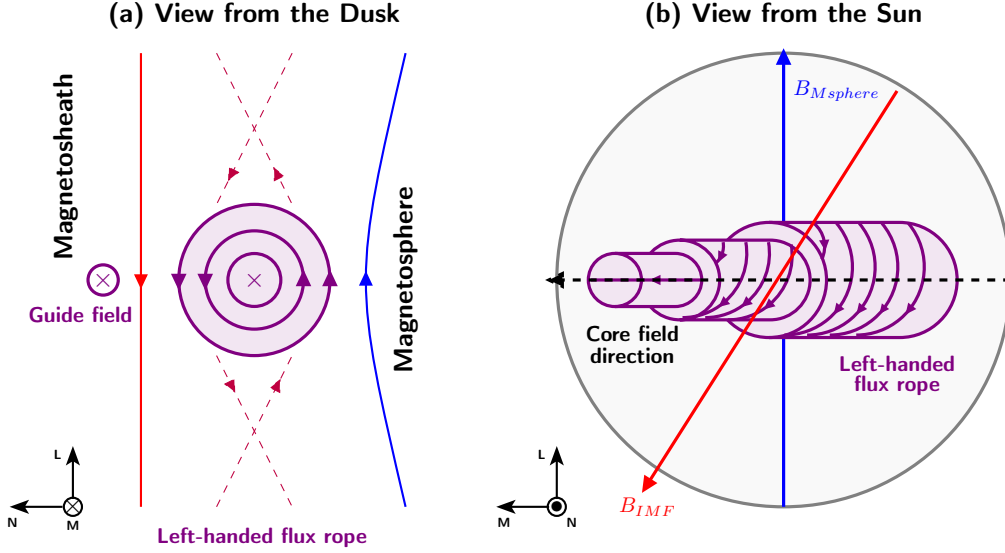


Figure 1. Schematic illustration of FTE formation by multiple X-line reconnection under a significant guide field. This illustration shows a dawnward and southward IMF leading to a dawnward core field and left-handed flux rope. Panel (a) shows a view from the dusk side and panel (b) shows a view from the sun. The FTE flux rope is represented in purple with arrows indicating the magnetic field direction. Solid blue and red lines represent magnetospheric and magnetosheath field lines, respectively. Adapted from Kieokaew et al. (2021).

160 The outline of this paper is as follows. Section 2 presents data from the Cluster and MMS
 161 missions and the methodology for event selection and flux rope fitting. Section 3 presents
 162 an example event from MMS and the statistical analyses of all events. Section 4 discusses
 163 our findings. Finally, Section 5 presents the conclusions and summary.

164 2 Data and methodology

165 2.1 Data overview

166 We utilize data from the Cluster (Escoubet et al., 2001) and MMS (Burch et al.,
 167 2016) missions. Cluster made observations at high latitudes ($|Z_{GSE}| > 5 R_E$), while
 168 MMS made observations at low latitudes ($-5 R_E < Z_{GSE} < 5 R_E$). We take data
 169 from Cluster 1 and Cluster 3. For MMS, we take data only from MMS 1 since all the
 170 MMS spacecraft observe identical features across FTE scale size.

171 For Cluster, we use the FTE list from Fear et al. (2012). The observations were
 172 made between November 2002 and June 2003 during the Cluster dayside season. We per-
 173 formed a visual inspection to determine the FTE time interval for each event. The cri-
 174 teria for selection are: (i) clear symmetric and bipolar variation of B_N (the magnetic field
 175 component perpendicular to the unperturbed magnetopause), and (ii) a clear enhance-
 176 ment in the magnetic field strength. For events observed using MMS, we obtained the
 177 list of quasi force-free FTEs from Kieokaew et al. (2021). This list is a subset of the FTE
 178 observations using MMS in 2015 to 2017 (Phases A and B) compiled by Fargette et al.
 179 (2020).

180 We use magnetic field measurements from the Flux Gate Magnetometer (FGM; Balogh
 181 et al., 2001) instrument on-board Cluster at 0.2 s resolution in the Geocentric Solar Eclip-
 182 tic (GSE) coordinate system. Similarly for MMS, we use magnetic field measurements
 183 from the FGM instrument on-board MMS (Russell et al., 2016) in both burst and sur-
 184 vey modes with resolutions of 0.01 s and 0.06 s, respectively. We use plasma moments
 185 consisting of ion bulk flow velocity, ion temperature, and ion number density from the
 186 Cluster Ion Spectrometry Hot Ion Analyser (CIS-HIA; Rème et al., 1997) instrument at
 187 about 4s resolution on-board Cluster, and the Fast Plasma Investigation (FPI; Pollock
 188 et al., 2016) measurements in both burst and survey modes with resolutions of 0.03 s/0.15
 189 s (electrons/ions) and 4.5 s, respectively. Finally, we use solar wind data from the OMNI
 190 database (King & Papitashvili, 2005), where the measurements were taken by the Ad-
 191 vanced Composition Explorer (ACE) and Wind spacecraft and time-shifted to the bow-
 192 shock nose, at 5-min resolution.

193 2.2 FTE observation

194 FTEs in spacecraft time-series data often exhibit clear signatures in the boundary
 195 normal coordinate system (LMN) (*e.g.*, Russell & Elphic, 1979). In the LMN system,
 196 \mathbf{N} is normal to the magnetopause and pointing outward from the Earth, \mathbf{M} the cross
 197 product of \mathbf{N} and the north geomagnetic dipole Z_{GSM} direction ($\mathbf{M} = \mathbf{N} \times \mathbf{Z}_{GSM}$),
 198 \mathbf{L} completes the right-handed orthonormal system. We adopt the magnetopause model
 199 from Shue et al. (1998) for locating the normal direction of the unperturbed magnetopause
 200 boundary. The Shue model describes the shape, size and location of the magnetopause
 201 boundary based on the function $r = r_0 \left(\frac{2}{1 + \cos \theta} \right)^{\alpha_{MP}}$, where r_0 is the stand-off distance
 202 of the magnetopause from the Earth, α_{MP} is the level of tail flaring, θ is the angle be-

203 tween the r_0 and r directions. r_0 and α_{MP} are empirical functions of the IMF B_z and
 204 the solar wind dynamic pressure (P_{dyn}), given as $r_0 = [10.22 + 1.29 \times \tanh(0.184 \times (B_z + 8.14))] \times$
 205 $P_{dyn}^{-1/6.6}$ and $\alpha_{MP} = (0.58 - 0.007 \times B_z) \times (1 + 0.024 \times \ln(P_{dyn}))$.

206 2.3 Flux rope fitting

207 To obtain the helicity sign of FTE flux ropes, we fit the data to a force-free model
 208 derived by Burlaga (1988), which was originally introduced to describe the magnetic field
 209 structure of magnetic clouds in the solar wind. The model is a solution of the cylindri-
 210 cally symmetric force-free configuration satisfying the equation $\nabla \times \mathbf{B} = \alpha \mathbf{B}$, where
 211 \mathbf{B} is the magnetic field and α is a constant, found by Lundquist (1950). The solution
 212 is found to be: $B_A = B_0 J_0(\alpha R)$ for the axial component, $B_T = B_0 H J_1(\alpha R)$ for the
 213 tangential component and $B_R = 0$ for the radial component, where $H = \pm 1$ is the
 214 helicity sign, R is the radial distance from the axis, J_0 and J_1 are the zeroth and first
 215 order Bessel functions of first kind, respectively, and B_0 is the maximum magnetic field
 216 strength inside the flux rope.

217 As introduced in Burlaga (1988), the model fitting is done in a local flux rope frame
 218 $(\mathbf{x}_v, \mathbf{y}_v, \mathbf{z}_v)$ (see Figure S1 of Kieokaew et al. (2021), adapted from Figure 2 of Burlaga
 219 (1988)). We use a more adapted frame similar to that used in Lepping et al. (1990). We
 220 take \mathbf{x}_v to be along the direction opposite to the flux rope motion such that $\mathbf{x}_v = -\mathbf{V}_{av}/|\mathbf{V}_{av}|$,
 221 where \mathbf{V}_{av} is the average flow velocity across the flux rope. We define $\mathbf{z}_v = \mathbf{n}$, where
 222 \mathbf{n} is the normal to the model magnetopause and \mathbf{y}_v completes the right-handed orthonor-
 223 mal system, *i.e.*, $\mathbf{y}_v = \mathbf{z}_v \times \mathbf{x}_v$. The five parameters describing the flux rope configu-
 224 ration in a local flux rope frame $(\mathbf{x}_v, \mathbf{y}_v, \mathbf{z}_v)$ are: (i) $\theta_0 \in [-90^\circ, 90^\circ]$ the angle between
 225 the flux rope axis and the ecliptic plane, (ii) $\phi_0 \in [0^\circ, 180^\circ]$ the angle between the ax-
 226 ial direction of the flux rope projected on the ecliptic plane and \mathbf{x}_v , (iii) b_0 the distance
 227 between the spacecraft and the flux rope motion plane, (iv) t_0 the time that corresponds
 228 to the closest approach of the flux rope to the spacecraft and (v) α is a constant. The
 229 helicity sign H is determined from magnetic field data. Nevertheless, we confirm the he-
 230 licity sign based on the quality of the resulting fit. As not all flux ropes can be assumed
 231 force-free, the quality of the fit is not always good. Here we select only flux ropes that
 232 can be fitted well to the model (*i.e.*, quasi force-free), and for which there is no ambi-
 233 guity on the helicity sign. We select 82 events from Cluster and 84 from MMS. Table
 234 S1 of the supplementary information for this work lists the 82 events from Cluster with

235 their respective start and end times, their locations in the GSE system and their helic-
 236 ity signs. The MMS events may be found in Table S1 of Kieokaew et al. (2021).

237 3 Event illustration & statistical analyses

238 3.1 Event overview

239 Figure 2 shows an example of an FTE, detected by MMS1 on November 5th, 2015,
 240 between 14:07:07 and 14:07:44 UT. It shows a 10-min interval (top) and a zoom-in (1-
 241 min interval; bottom). Panels (a) and (a') present the magnetic field in the GSE coor-
 242 dinate system and its magnitude $|\mathbf{B}|$. Panel (b') present the components of the magnetic
 243 field in the $(\mathbf{x}_v, \mathbf{y}_v, \mathbf{z}_v)$ frame. Panel (b) shows the components of the ion velocity in the
 244 GSE coordinate system. Panel (c) displays the ion number density. Panel (d) shows the
 245 ion temperature in the direction parallel and perpendicular to the magnetic field. Panel
 246 (e) presents the ion energy spectrogram. The bipolar signature of the flux rope is vis-
 247 ible in panels (a) as shaded in gray, but it is most clearly seen in panel (b') where the
 248 B_{z_v} component rotates from negative to positive. We also observe an enhancement in
 249 the magnetic field strength in panel (a) and (a') during this bipolar variation. In addi-
 250 tion, we also observe a slight increase in the temperature in panel (d) during the flux rope
 251 interval. The dashed lines in panel (b') represent the flux rope model fit during the flux
 252 rope time interval. In this case, the better fit was found for $H = -1$. Therefore, this
 253 flux rope twist is categorized as left-handed (LH). To understand the local conditions
 254 surrounding this flux rope, we also characterize the adjacent magnetospheric and mag-
 255 netosheath regions as follows. The region highlighted in red in panels (a) to (e) shows
 256 the magnetosphere region adjacent to the flux rope, which is marked between 14:13:45
 257 and 14:14:00 UT. This region is identified by an almost instantaneous drop in the ion
 258 number density seen in panel (c) co-located with a dropout in the fluxes of low energy
 259 (< 1 keV) ions, and with intense fluxes of higher energy ions (> 1 keV) that is distinct
 260 from the surrounding regions. The region highlighted in green shows the magnetosheath
 261 region most adjacent to the flux rope, between 14:06:40 and 14:06:55 UT. This region
 262 is identified with the larger density and lower temperature.

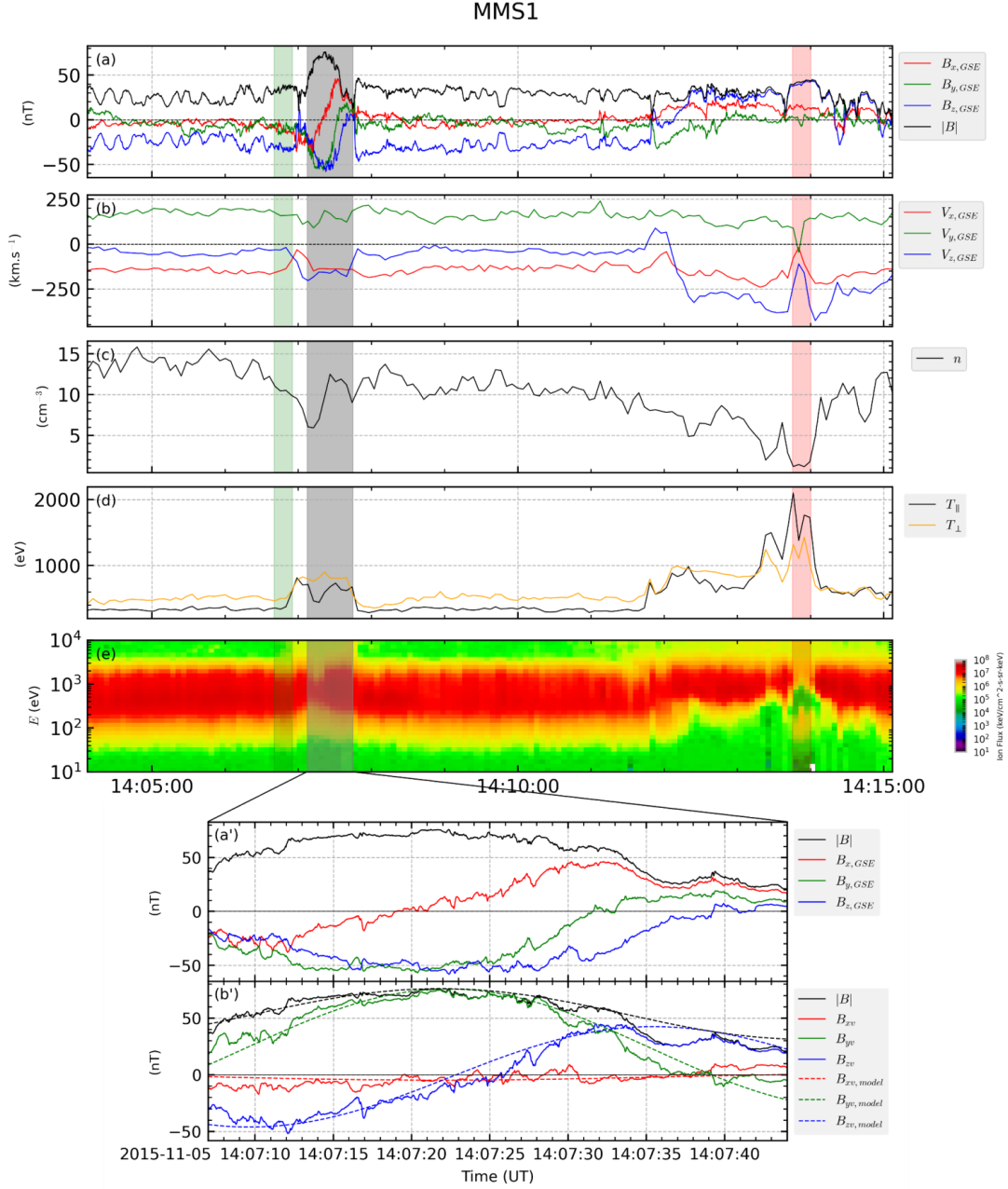


Figure 2. MMS observations of an FTE shown for a 10-min interval (top; panels (a) to (e)) and a 1-min interval (bottom; panels (a') and (b')). The FTE is highlighted in gray in the top panels. Panels (a) show the magnetic field in the GSE coordinate system. Panels (b), (c), (d) show the ion bulk velocity in the GSE coordinate system, the ion number density, and the ion temperature, respectively. Panel (e) shows the ion energy spectrogram. The green and red shaded regions mark the adjacent magnetosheath and magnetospheric regions to the FTE, respectively. Panels (a') and (b') show the zoom-in of the panels (a) in GSE and (x_v, y_v, z_v) coordinates system, respectively.

3.2 Spatial distribution

Figure 3 shows the spatial distribution of all the events in the GSE coordinate system. Crosses represent RH ($H = +1$) flux ropes and triangles represents LH ($H = -1$) flux ropes. Panel (a) shows a projection in the $Y_{GSE}-Z_{GSE}$ plane as viewed from the Sun (positive X_{GSE}), and panel (b) is a projection in the $X_{GSE}-Y_{GSE}$ plane as viewed from the north (positive Z_{GSE}), with the approximate magnetopause boundary using the average IMF B_z and P_{dyn} from the Shue model. The MMS events are located in the low latitude region, while Cluster events are located at higher latitudes and further from the nose. There are more events on the dusk side (positive Y_{GSE}) than on the dawn side. From our investigation, these events are often found downstream of quasi-perpendicular shocks, where the magnetosheath data are often more laminar (which lead to an easier identification of FTEs). Nevertheless, there is no spatial preferences for the RH and LH flux ropes as they appear to be distributed almost uniformly across the planes.

3.3 Solar wind conditions

To revisit the correlation between the IMF B_y and the FTE helicity sign, we analyse the IMF conditions preceding the detection of the FTEs, which would affect the local conditions in which magnetic reconnection takes place on the dayside magnetopause. As OMNI data provide solar wind conditions at the nose of the bowshock, we estimate the propagation time of the solar wind flow to be approximately 15 minutes to cross the magnetosheath and reach the magnetopause. The results are not sensitive with intervals between 15 and 30 minutes.

Figure 4 shows the distribution of the 15-min averaged IMF clock angles ($\theta_{CA} = \arctan(B_y/B_z)$) preceding the events in polar histograms. Panel (a) shows the distribution for RH events and panel (b) shows the distribution for LH events. Positive IMF clock angles ($0^\circ < \theta_{CA} < 180^\circ$) correspond to duskward IMF B_y , while the negative IMF clock angles ($-180^\circ < \theta_{CA} < 0^\circ$) correspond to dawnward IMF B_y . Figure 4 shows that the majority of RH events are preceded by positive IMF clock angles (IMF $B_y > 0$) as seen in panel (a), while the majority of the LH events are preceded by negative IMF clock angles (IMF $B_y < 0$) as seen in panel (b). This group where the FTE helicity sign corresponds to the IMF B_y is referred as the regular group. This group is consistent with a flux rope generation by the multiple X-line reconnection scenario as explained in Kieokaew

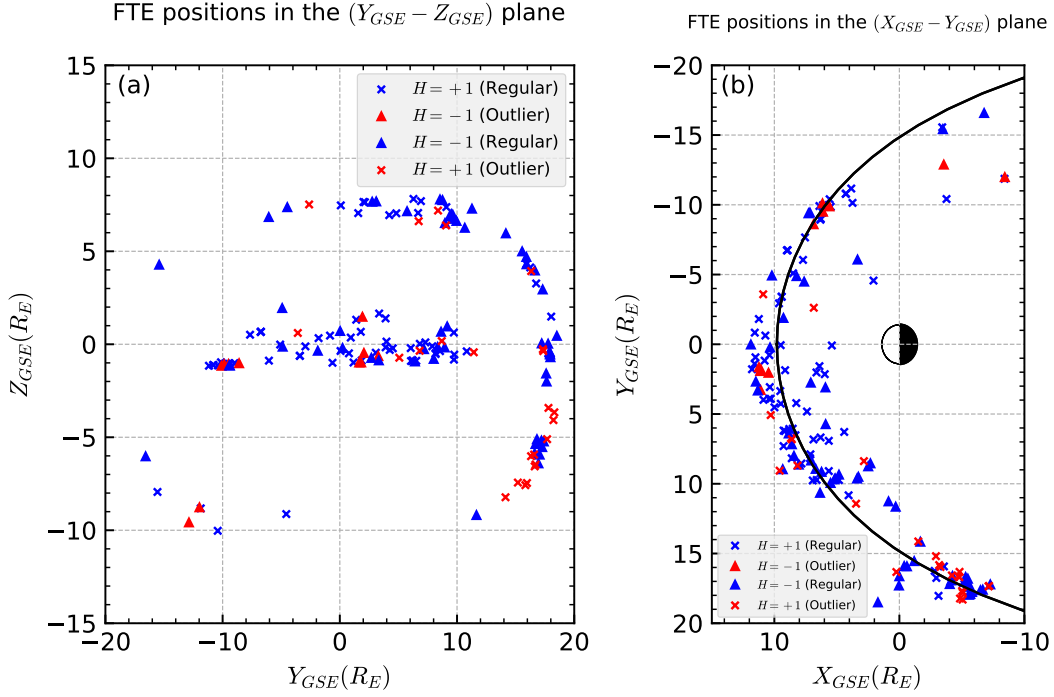


Figure 3. Spatial distribution of the FTEs in the GSE coordinate system in the (a) Y-Z and (b) X-Y planes. The RH ($H = +1$) events are denoted by crosses and the LH ($H = -1$) events are denoted by triangles. We distinguish the outlier events (in red) and regulars (in blue).

The solid black line in panel (b) represents the magnetopause boundary from the Shue model with $r_0 = 9.8 R_E$ and $\alpha_{MP} = 5.6$.

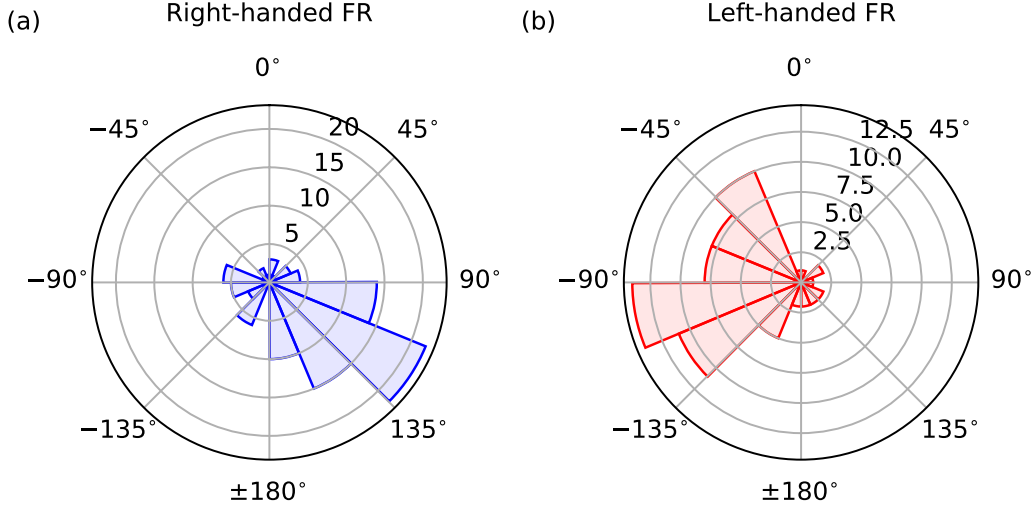


Figure 4. Distribution of the averaged IMF clock angle for (a) RH events, (b) LH events.

294 et al. (2021). However, in Figure 4, there are some events where the helicity sign does
 295 not correspond to the IMF B_y for both RH events and LH events. This group, in which
 296 we call the “outliers”, constitutes 21% of all events. We distinguish the spatial distri-
 297 bution of the outlier group with the red colour in Figure 3, while the regular group is
 298 presented in blue.

299 To investigate the solar wind conditions that might control the regular and out-
 300 lier events, we also investigate other parameters such as the ion bulk velocity, ion num-
 301 ber density, Mach number, and ion temperature. We do not find a correlation between
 302 those upstream parameters and the flux rope helicity sign. To investigate local effects,
 303 we investigate the conditions at the magnetopause where the FTEs may be generated.
 304 In particular, we focus on the local magnetic shear properties between the magnetosheath
 305 and the magnetospheric magnetic fields in the vicinity of the FTEs.

306 3.4 Local magnetic shear properties

307 As there is no clear correlation between the upstream solar wind parameters and
 308 the helicity sign of the outlier group, we now shift our focus to investigate local magne-
 309 topause properties. We employ two approaches to determine the local magnetic shear.
 310 First, we explore the model proposed by Trattner et al. (2007) that estimates the local
 311 shear angle across the magnetopause surface by assuming a draping of the IMF and the

312 local flow (Cooling et al., 2001). For a given averaged IMF clock angle for each FTE,
 313 we obtain a spatial distribution of the magnetic shear on the magnetopause surface. Fig-
 314 ure 5 shows the local, 2-D magnetic shear angle map for a given IMF clock angle at 225.5°
 315 (IMF cone angle at 99° and dipole tilt angle at -8°) on the magnetopause in the (Y_{GSM}, Z_{GSM})
 316 plane on November 5, 2015, at 14:07:07 UT; the black cross (at $Y = 5.5 R_E$, $Z = -3.4 R_E$)
 317 locates the position of the FTE. This approach allows us to model local magnetic shear
 318 at the FTE location, which may indicate the local condition in which the FTE is formed,
 319 *e.g.*, by magnetic reconnection near the location of the FTE. Figure 6 shows a histogram
 320 of the distribution of the magnetic shear angle modelled at the FTE location for all 166
 321 events. We categorize the data into the regular and outlier groups, represented by solid
 322 black and dashed red lines, respectively. We find that the majority of the outlier group
 323 has large magnetic shears with the events being mainly around 150° . In contrast, we find
 324 that the regular flux ropes have a broader distribution centered around moderate mag-
 325 netic shear angles.

326 To check whether the magnetic shear angles from the model are consistent with
 327 the observed shear properties, we also obtain local shear angles using the data surround-
 328 ing the outlier flux ropes. The procedure is as follows. We select two regions, one in the
 329 magnetosphere and one in the magnetosheath. The magnetosphere has low density but
 330 high temperature, while the magnetosheath has a larger density and lower temperature.
 331 We avoid strong current layers, regions with jets, accelerated particles or other flux ropes,
 332 throughout the selection process. We find that most of the flux ropes are found on the
 333 magnetosheath side in the observations. We select a magnetosheath region and a mag-
 334 netosphere region that are adjacent or close to the studied flux rope. The magnetosphere
 335 is generally found from 1-min to 1-hour away from the flux rope (Figure 2). We calcu-
 336 late the shear angle by calculating $\arccos\left(\frac{\mathbf{B}_{sp} \cdot \mathbf{B}_{sh}}{|\mathbf{B}_{sp}| |\mathbf{B}_{sh}|}\right)$, where \mathbf{B}_{sp} is the magnetic field
 337 vector in the magnetosphere, and \mathbf{B}_{sh} is the magnetic field vector in the magnetosheath.
 338 The results are also shown in Figure 6 as denoted by the dashed blue line. The magnetic
 339 shear angles obtained from this alternative method are consistent with the results from
 340 the modeling.

341 4 Discussion

342 We have investigated the helicity sign of 166 quasi force-free FTEs, with 82 from
 343 Cluster and 84 from MMS observations. We found that the helicity sign of most events

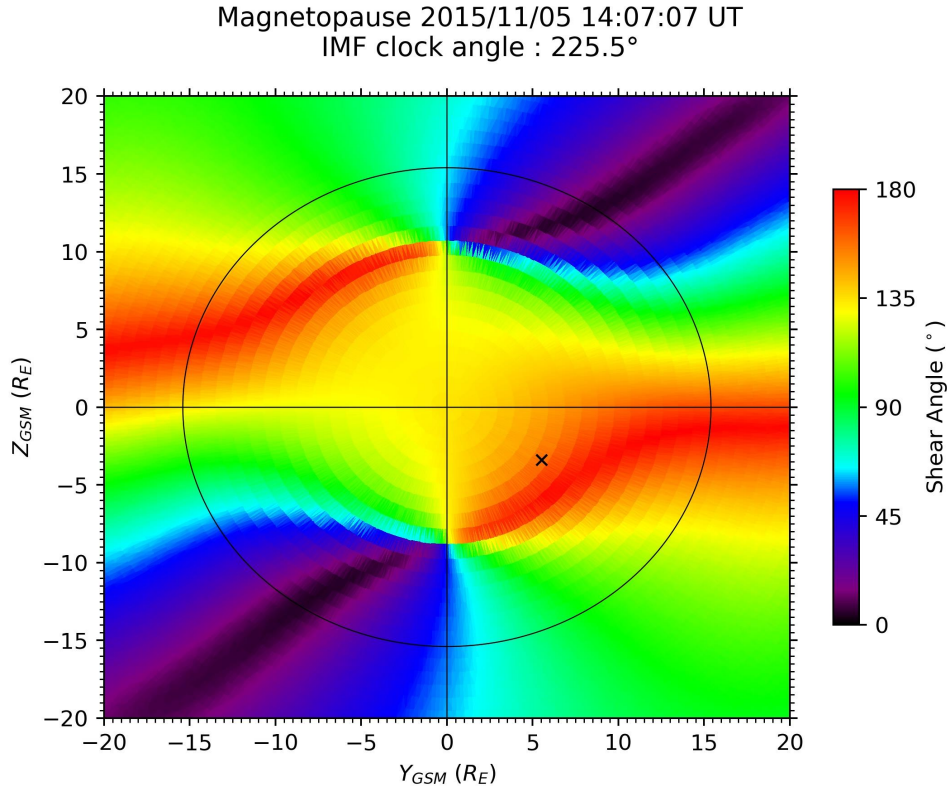


Figure 5. The magnetic shear angle map at the magnetopause surface projected onto the Y - Z plane of the GSM coordinate system. The map is obtained for the event in Figure 1 on November 5th, 2015 at 14:07:07 UT produced using the averaged IMF clock angle (at 225.5°) preceding the event. The color scale represents the local magnetic shear angle from 0° (dark purple; no shear) to 180° (red; highest shear). The black cross marks the FTE location. The black circle denotes the terminator ($X_{GSM} = 0$).

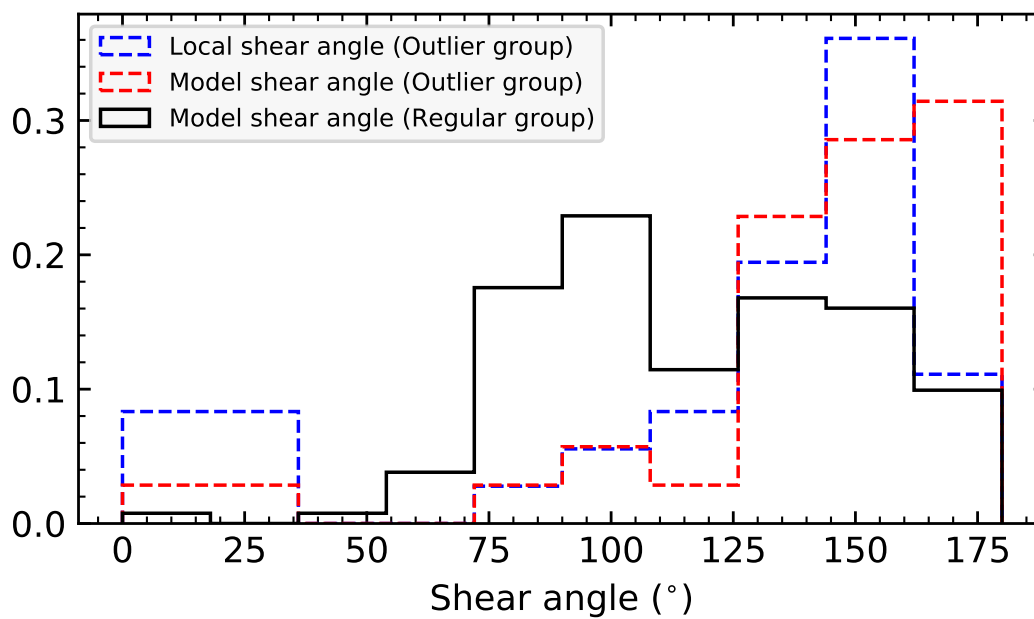


Figure 6. Distributions of the magnetic shear angle associated with the FTEs. The distributions of regular and outlier groups obtained from the model (Trattner et al. (2007)) are shown with black solid and red dashed lines, respectively. The distribution of the outlier group obtained from in-situ data is shown in blue dashed line. The distributions are normalized to the total number of each group.

344 is ordered by the IMF B_y polarity, and so that positive IMF clock angles correspond to
 345 duskward IMF B_y , while negative IMF clock angles ($-180^\circ < \theta_{CA} < 0^\circ$) correspond
 346 to dawnward IMF B_y . We also found that 21% of the events have a helicity sign that
 347 does not correspond to the expected IMF B_y polarity. Our findings are consistent with
 348 the main results of Kieokaew et al. (2021), where right-handed FTEs are associated with
 349 positive IMF B_y and left-handed FTEs are associated with negative IMF B_y . To inves-
 350 tigate the local conditions associated with the FTE formation, we analysed the magnetic
 351 shear angle using both modelling and in-situ data at the FTE locations. We found that
 352 the majority of the outlier FTEs (those whose expected helicity does not correspond to
 353 the IMF B_y polarity) are located in generally higher magnetic shear regions.

354 As a first simple explanation, for a given small IMF B_y the determination of the
 355 core field and helicity sign at low guide field (e.g., for high shears) may be more random
 356 because of the uncertainties in mapping the IMF observations to the magnetopause (mak-
 357 ing the helicity - IMF B_y relation less clear at low guide field). In the absence or the pres-
 358 ence of a finite low guide field, Karimabadi et al. (1999) demonstrated using hybrid sim-
 359 ulations that the Hall magnetic field plays a key role in determining the core field of flux
 360 ropes. Similar to their conclusions, we propose that the core field and associated heli-
 361 city sign of outlier FTEs are explained by the interplay between the Hall and guide fields
 362 (e.g., Aunai et al., 2011), during low guide field conditions, rather than just randomness,
 363 as explained next.

364 Our findings in Figure 6 show that the outlier flux ropes (shown in red and in blue)
 365 are mostly characterised by high magnetic shears (125° to 180°), while the regular flux
 366 ropes (shown in black) show a broad distribution with a maximum value around mod-
 367 erate magnetic shears ($\sim 100^\circ$). This finding suggests that the core field and helicity sign
 368 of flux ropes is affected by the local magnetic shear properties in their vicinity. Assum-
 369 ing the magnetic shear at the FTE generation site is not too different from that at their
 370 observed locations, we may consider a core field and thus helicity generation mechanism
 371 as follows. In the presence of a significant guide field, e.g., at moderate shear angle, the
 372 core field and the helicity sign of the generated FTE are likely determined by the guide
 373 field of magnetic reconnection (e.g., Karimabadi et al., 1999). Since the IMF B_y is the
 374 main component that provides the reconnection guide field under southward IMF con-
 375 ditions, the helicity sign of the produced FTE therefore corresponds to the IMF B_y po-
 376 larity. This mechanism may explain the regular flux ropes found in our study and in Kieokaew

377 et al. (2021). In the presence of a weak guide field, *e.g.*, at higher magnetic shear, how-
378 ever, the determination of the FTE core field and helicity appears less clear. We now ex-
379 plain in more details how the Hall physics of magnetic reconnection in the absence of
380 guide field may determines the core field and helicity sign of FTE flux ropes.

381 Near the X-line of anti-parallel magnetic reconnection, *i.e.*, in the ion diffusion re-
382 gion, the Hall electric field is produced as ions meander around the magnetic null while
383 electrons remain frozen-in. Under symmetric inflow conditions, this Hall electric field drags
384 out the newly reconnected magnetic fields and produces a quadrupolar pattern in the
385 out-of-plane (guide field) direction (*e.g.*, Mandt et al., 1994; Nagai et al., 2001; Borg et
386 al., 2005; Denton et al., 2016). At the dayside magnetopause, magnetic reconnection is
387 asymmetric due to the denser plasma in the magnetosheath. Thus, the Hall field pat-
388 tern on the magnetosheath side dominates and leads to a more bipolar Hall pattern (*e.g.*,
389 Karimabadi et al., 1999; Eastwood et al., 2013; Y. C. Zhang et al., 2017). Since the out-
390 lier events are mostly found for high magnetic shears, we expect that their core field, and
391 in turn their helicity, is determined by the Hall field, consistent with previous works by
392 Karimabadi et al. (1999), Teh, Abdullah, and Hasbi (2014) and Teh, Nakamura, et al.
393 (2014).

394 To summarize the process explained above, Figure 7 shows a schematic of FTE flux
395 rope generation in asymmetric magnetic reconnection under magnetopause-like condi-
396 tions. Panel (a) shows conditions without a guide field, *i.e.*, anti-parallel reconnection,
397 while panel (b) shows the conditions with a guide field, *i.e.*, component reconnection.
398 The solid black lines denote the projection of magnetic field lines and the dashed black
399 lines denote the separatrices, with black arrows indicating their directions. We mark the
400 plasma inflow with an orange arrow and the plasma outflows with green arrows. The Hall
401 pattern is represented by the circles with crosses or dots on the separatrices indicating
402 the in- and out- of-plane magnetic field directions, respectively. In panel (a), the guide
403 field is absent (or weak), and the Hall magnetic field pattern is more dominant on the
404 magnetosheath side than the magnetospheric side due to the denser plasma (Mozer &
405 Hull, 2010); we denote this dominant Hall field with the bigger circles. In this case, the
406 Hall pattern on the magnetosheath side determines the core field of the flux ropes, and
407 in turn the helicity; they are represented by the thick blue and red circles. In panel (b),
408 however, the presence of a significant guide field reverses the effect of the Hall field and/or,
409 to first order, adds up with it to determine the core field and helicity of the FTEs. They

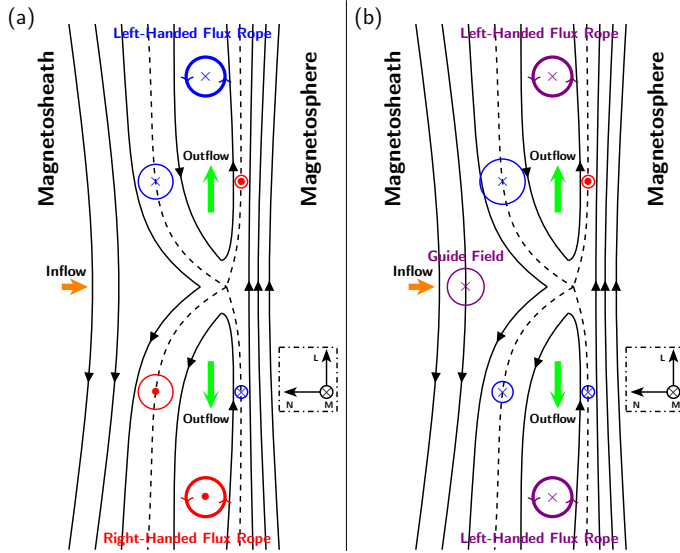


Figure 7. Schematic illustration of (a) anti-parallel and (b) component or guide field magnetic reconnection. Solid black lines represent the magnetic field lines and the dashed black lines represent the separatrices. Blue and red circles represent the Hall pattern, with their sizes corresponding to the magnitude of the Hall field which is stronger in the magnetosheath side due to the asymmetry in the inflow plasma density. In panel (b), the purple circle represents the guide field. The thicker circles represent the flux ropes generated in the reconnection exhausts. Green arrows represent the reconnection outflow, while orange arrows represent the inflow. We note that these illustrations focus on the role of the Hall field at the dominant X-line and thus do not represent the complete FTE helicity generation that involves multiple X-line reconnection (see text).

are illustrated with purple circles, *e.g.*, for inward guide field. In brief, these simplified scenarios explain how the FTEs generate their core fields under anti-parallel (high shear) and component (moderate shear) magnetic reconnection (Karimabadi et al., 1999), leading to helicity signs as reported in our study. To further support this scenario, we include results from the simulation previously published by Chen et al. (2020) as outlined next.

The present study corroborates previous work on FTE core field generation as a result of the Hall pattern. While to our knowledge our study is the first statistical analyses of in-situ observations of this process, previous simulations by Karimabadi et al. (1999) originally proposed such a mechanism. Figure 8 shows simulation results from the MHD

420 with embedded particle-in-cell (MHD-EPIC) model with a purely southward IMF con-
 421 dition (no guide field) published by Chen et al. (2020). The color scale shows the out-
 422 of-plane magnetic field intensity (B_y component) projected onto the $X-Z$ plane of the
 423 GSM system, *i.e.*, as viewed from the dawn side. Panels (a) and (b) show the time evo-
 424 lution of FTE generation due to sequential reconnection X-line formation. The box de-
 425 lined by a black line represents the region that is simulated using the PIC code to in-
 426 clude the kinetic physics of magnetic reconnection. Here, panel (a) shows the first re-
 427 connection X-line formation as marked by a red star. The polarity of B_y north and south
 428 of the X-line shows negative and positive values, respectively. This bipolar B_y variation
 429 is the bipolar Hall pattern produced as a consequence of asymmetric reconnection with
 430 the denser plasma in the magnetosheath side. Panel (b) shows the simulation about 7
 431 minutes later when the first X-line has propagated northward while the second and the
 432 third reconnection X-lines sequentially appear as marked with gray stars. Between the
 433 first and second X-lines in panel (b), as zoomed-in in panel (c), an FTE bounded by a
 434 white contour forms. The key observation here is that the core field of this FTE retains
 435 the Hall pattern of the two X-lines. In other words, panel (c) illustrates an example of
 436 how an FTE generates its core field from the Hall magnetic field of magnetic reconnection.
 437 Additionally, panel (d) shows a zoom-in of the second and third X-lines. Here, an-
 438 other FTE with the same core field as generated by the initial Hall perturbation is also
 439 being formed. Despite the Hall magnetic field perturbation, the formation of the FTEs
 440 follows the standard mechanism proposed by Raeder (2006) under large dipole tilt an-
 441 gles, where an FTE can be generated between multiple X-lines. Based on our statistical
 442 results and this simulation work, we conclude that the outlier FTE core fields and en-
 443 suing helicity are determined from the Hall magnetic field of magnetic reconnection for
 444 a weak guide field condition. In brief, the Hall magnetic field leads to the core field and
 445 thus the helicity sign of FTEs in the absence of a guide field.

446 In magnetic reconnection, the Hall field intensity is likely determined by the inflow
 447 plasma properties (*e.g.*, Le et al., 2009), and the Hall structure may be controlled by the
 448 Alfvén speed profile in asymmetric reconnection (Dai, 2018). The properties of recon-
 449 nection Hall field may consequently control the core field of FTEs in a low guide field
 450 environment, a possibility that deserves to be investigated in the future. In Figure 6, we
 451 find that the outlier flux rope becomes dominant over the regular flux rope distribution
 452 for magnetic shears higher than about 125° . This behavior suggests that the Hall field

453 starts to dominate over the guide field in determining the final flux rope helicity at about
454 such a value. To first order, assuming a symmetric magnetic field (such that for the same
455 reconnecting field component the guide field is the same on both sides of the reconnect-
456 ing current sheet), a shear angle of 125° corresponds to a ratio between the guide field
457 and reconnecting field of about 0.5. For lower guide field, the effect of the Hall magnetic
458 field thus becomes statistically dominant. This is an approximation, and depending on
459 local conditions, as well as remote conditions near the initial reconnection site, the ex-
460 act value of the magnetic shear at which a given effect becomes dominant may vary. Our
461 analysis in Figure 6 also shows a small but non-negligible number of FTEs with small
462 shear angles. It is thus possible that these FTEs have propagated from elsewhere where
463 the local conditions have a higher shear, further showing that the suggestive shear value
464 of $\sim 125^\circ$ for separating the effects of the Hall and guide fields is very approximate.

465 The generation of FTEs by multiple X-lines is not just an assumption in our study
466 (see Figure 1 and Section 1) as it is in fact the only valid paradigm to interpret our re-
467 sults. Indeed, considering the role of the Hall magnetic field in determining both the core
468 field and helicity sign of flux ropes, under low guide field, the single X-line formation mech-
469 anism would always create a left-handed flux rope northward of the reconnection site and
470 a right-handed flux rope southward of the reconnection site, as shown in Figure 7a. If
471 it were the case, this would lead to a systematic north-south dichotomy in left-handed
472 and right-handed flux ropes for the outlier group (which occur for low guide field), while
473 this is not observed in-situ. In particular this trend is not observed in Figure 3 where
474 the red crosses and triangles denote the outlier flux ropes (respectively right- and left-
475 handed). Our findings thus support the idea that FTE flux ropes are produced through
476 a multiple X-line mechanism.

477 So far our discussion on the role of the Hall magnetic field in determining the core
478 field neglected the fact that we are adopting multiple X-line reconnection as a forma-
479 tion mechanism of FTEs. There should be two distinct Hall patterns that would be present
480 at the two X-lines surrounding the FTE flux rope, and that may affect the internal mag-
481 netic structure of the FTE. In other words, the Hall pattern is present in the exhausts
482 of the two X-lines surrounding the FTE flux rope. In a low guide field scenario, one of
483 the two Hall signatures may determine the core field of the FTE flux rope. But this raises
484 the question of which X-line is dominant or which X-line controls the core field and he-
485 licity sign of the flux rope. Different parameters could come into play to determine which

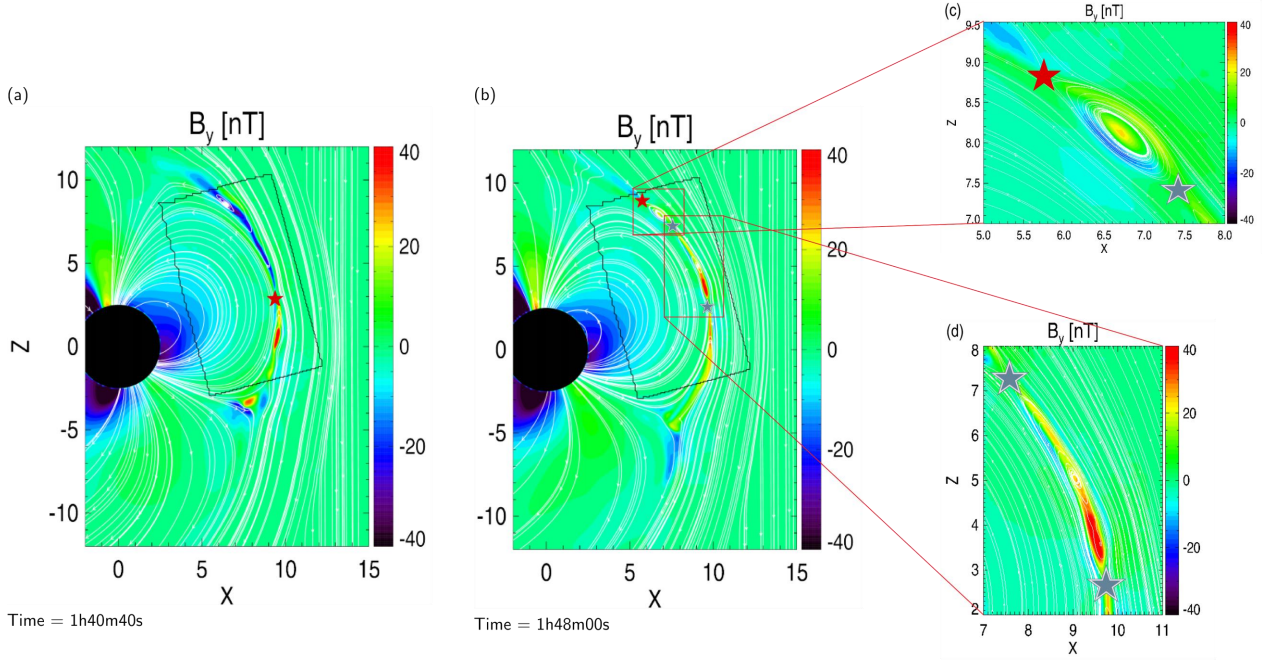


Figure 8. The evolution of the dayside magnetopause using a global MHD simulation embedded with PIC code for the area delineated by a black square. The simulation shows the magnetic field B_y component in the $X - Z$ plane in the GSM coordinate system as viewed from the dawn side. Panel (a) shows a snapshot where a reconnection X-line is first formed as marked by a red star. Panel (b) shows a snapshot around 7 minutes later of panel (a) where the second and third X-lines, marked by gray stars, are now formed. Panel (c) shows a zoom-in of an FTE formation between the first and the second X-lines. Panel (d) shows a zoom-in of another FTE formation between the second and the third X-lines.

486 X-line Hall field become dominant. In particular, the simulation shown in Figure 8 sug-
 487 gest that the initial X-line Hall pattern may be dominant. Indeed, the Hall pattern of
 488 the initial X-line (represented by a red star in Figure 8) gives the core field and helic-
 489 ity sign of the FTEs generated later in the simulation, as shown in Figures 8c and 8d.
 490 Thus the temporal sequence of X-line formation should play an important role in the de-
 491 termination of the flux rope core field and the helicity sign. Nevertheless, this conclu-
 492 sion comes from only one simulation. More dedicated studies are required to confirm whether
 493 this conclusion is general. In particular, one may expect that, in addition to the tem-
 494 poral sequence, the reconnection rate at each X-line may have an impact on which Hall
 495 field pattern may eventually dominate the flux rope topology. Moreover, we note that

496 an FTE formation may be a continuous process where dynamical processes such as
497 coalescence, erosion, and division due to active magnetic reconnection can influence FTE
498 structures (*e.g.*, Akhavan-Tafti et al., 2019, 2020). The core field of an FTE may thus
499 be an accumulative effect of multiple reconnection with a varying reconnection rate de-
500 pending on solar wind conditions, as well as the complex FTE evolution due to ongo-
501 ing reconnection. All these aspects deserve to be further investigated but they are be-
502 yond the scope of our study.

503 5 Summary and conclusions

504 We performed a statistical study of the helicity sign of 166 quasi force-free FTEs,
505 82 of which were observed by Cluster, and 84 by MMS. We found that the helicity sign
506 of the majority of the events corresponds to the IMF B_y polarity; this population is called
507 the regular group. However, we also found that the helicity sign of a significant num-
508 ber of events (21% of the total events) does not correspond to the IMF B_y polarity; this
509 population is called the outlier group. To better understand the formation of regular and
510 outlier FTEs, we investigated the local properties of the magnetopause surrounding the
511 FTE locations. In particular, we modeled, based on the Maximum Magnetic Shear model
512 by Trattner et al. (2007), the local magnetic shear angle for each FTE. We found that
513 the regular group show a spread distribution with a maximum value around moderate
514 shear angles. For moderate and low shear angles, the guide field expected at the recon-
515 nection sites, where FTEs were formed, would control the core field of FTEs, and thus
516 the helicity sign. This situation is consistent with the fact that the IMF B_y controls the
517 helicity sign of the regular group as the IMF B_y represents the main component that pro-
518 vides the reconnection guide field (Kieokaew et al., 2021). For the outlier group, in ad-
519 dition to the model, we have investigated the shear angle using in-situ data surround-
520 ing each outlier FTE. We found that they are observed at higher magnetic shear loca-
521 tions meaning lower guide field closer to the reconnection sites. In this case, it is less clear
522 what controls the core field of the outlier FTEs. In particular, there are higher uncer-
523 tainties on the IMF mapping and therefore a higher randomness may be expected in the
524 determination of helicity and core field under low guide field at the reconnection site.
525 However, under such conditions, another physical process may be at work. Using hybrid
526 simulations, Karimabadi et al. (1999) originally demonstrated that the Hall effect in the
527 reconnection site may control the core field of FTEs. They also discussed that plasma

528 β and the presence of a pre-existing guide field are two important controlling parame-
529 ters of the Hall-generated field. Our statistical analyses here are consistent with their
530 results regarding the control of the FTE core field by the Hall field in a low guide-field
531 (*i.e.*, high magnetic shear) environment.

532 At the magnetopause, anti-parallel magnetic reconnection is typically triggered un-
533 der asymmetric plasma conditions. In this case, the Hall magnetic field has a strongly
534 skewed quadrupolar pattern, so that the pattern looks mostly bipolar with the Hall field
535 in the two exhausts having opposite out-of-plane orientations (Figure 7). We propose
536 that this bipolar Hall pattern in turn controls the core field of FTE flux ropes, and thus,
537 controls their helicity sign. The effect was shown using the results from a global MHD
538 simulation with embedded PIC code (Chen et al., 2020), reproduced here in Figure 8.
539 Our study also supports the multiple X-line mechanism for the process to produce FTEs
540 as we do not observe any north-south dichotomy for the right-handed and left-handed
541 flux ropes for the outlier group, which occurs for low guide field, while under such con-
542 ditions a generation mechanism based on a single X-line would suggest such a dichotomy
543 between hemispheres. The presence of two X-lines in the vicinity of FTE flux ropes means
544 the existence of two distinct Hall patterns from the two X-lines surrounding the FTE,
545 but only one of them should dominate and determine the core field and helicity of FTEs.
546 For instance, in the case of Figure 8 we find that the initial X-line is dominant and thus
547 the temporal sequence of X-line formation appears to play an important role in deter-
548 mining the dominant Hall effect on subsequent FTE formation. Future work should look
549 into this temporal sequence of X-line formation, and its contribution in determining the
550 dominant Hall field. Of course, attention should also be given to the reconnection rate
551 which should also come into play, in addition to the temporal sequence. Furthermore,
552 the dynamical, complex FTE evolution due to ongoing reconnection at the surrounding
553 X-lines may influence the FTE structures as they propagate. This work highlights an
554 important aspect of the fundamental interconnection between kinetic scale processes of
555 magnetic reconnection and the macroscale structures of FTEs.

556 **Data availability information**

557 MMS, Cluster and OMNI data are available online at [https://lasp.colorado.edu/](https://lasp.colorado.edu/mms/sdc/public/)
558 [mms/sdc/public/](https://lasp.colorado.edu/mms/sdc/public/), <https://csa.esac.esa.int/csa-web/> and [https://omniweb.gsfc](https://omniweb.gsfc.nasa.gov/)
559 [.nasa.gov/](https://omniweb.gsfc.nasa.gov/), respectively.

Acknowledgments

Work at IRAP was supported by CNRS, CNES and UPS. Our analysis made use of the tools developed at IRAP by the CDDP (AMDA <http://amda.cdpp.eu/>, and speasy <https://pypi.org/project/speasy/>) and by E. Penou (CL, <http://clweb.irap.omp.eu/>). CDDP, the Centre de Données de la Physique des Plasmas, is supported by CNRS, CNES, Observatoire de Paris and Université Paul Sabatier, Toulouse. R. C. Fear received funding from Science and Technology Facilities Council Consolidated Grant ST/ V000942/1.

References

- Akhavan-Tafti, M., Palmroth, M., Slavin, J. A., Battarbee, M., Ganse, U., Grandin, M., ... Stawarz, J. E. (2020). Comparative analysis of the vlsiator simulations and mms observations of multiple x-line reconnection and flux transfer events. *Journal of Geophysical Research: Space Physics*, *125*(7), e2019JA027410. Retrieved from <https://agupubs.onlinelibrary.wiley.com/doi/abs/10.1029/2019JA027410> (e2019JA027410 2019JA027410) doi: <https://doi.org/10.1029/2019JA027410>
- Akhavan-Tafti, M., Slavin, J. A., Sun, W. J., Le, G., & Gershman, D. J. (2019). MMS Observations of Plasma Heating Associated With FTE Growth. *Geophysical Research Letters*, *46*(22), 12654–12664. doi: 10.1029/2019GL084843
- Aunai, N., Retinò, A., Belmont, G., Smets, R., Lavraud, B., & Vaivads, A. (2011). The proton pressure tensor as a new proxy of the proton decoupling region in collisionless magnetic reconnection. *Annales Geophysicae*, *29*(9), 1571–1579. Retrieved from <https://angeo.copernicus.org/articles/29/1571/2011/> doi: 10.5194/angeo-29-1571-2011
- Balogh, A., Carr, C. M., Acuña, M. H., Dunlop, M. W., Beek, T. J., Brown, P., ... Schwingenschuh, K. (2001). The Cluster Magnetic Field Investigation: overview of in-flight performance and initial results. *Annales Geophysicae*, *19*(10/12), 1207-1217.
- Berger, M. A. (1982). Rapid reconnection and the conservation of magnetic helicity. *Bulletin of the American Astronomical Society*, *15*.
- Berger, M. A. (1984). Magnetic helicity: Gauge-invariant formulation and conservation properties. *Bulletin of the American Astronomical Society*, *16*.
- Berger, M. A. (1999, dec). Introduction to magnetic helicity. *Plasma Physics and*

- 592 *Controlled Fusion*, 41(12B), B167–B175. Retrieved from <https://doi.org/10>
593 [.1088/0741-3335/41/12b/312](https://doi.org/10.1088/0741-3335/41/12b/312) doi: 10.1088/0741-3335/41/12b/312
- 594 Berger, M. A., & Field, G. B. (1984). The topological properties of mag-
595 netic helicity. *Journal of Fluid Mechanics*, 147, 133–148. doi: 10.1017/
596 S0022112084002019
- 597 Borg, A. L., Øieroset, M., Phan, T. D., Mozer, F. S., Pedersen, A., Mouikis,
598 C., ... Rème, H. (2005). Cluster encounter of a magnetic reconnec-
599 tion diffusion region in the near-earth magnetotail on september 19,
600 2003. *Geophysical Research Letters*, 32(19). Retrieved from [https://](https://agupubs.onlinelibrary.wiley.com/doi/abs/10.1029/2005GL023794)
601 agupubs.onlinelibrary.wiley.com/doi/abs/10.1029/2005GL023794 doi:
602 <https://doi.org/10.1029/2005GL023794>
- 603 Bothmer, V., & Schwenn, R. (1998). The structure and origin of magnetic clouds
604 in the solar wind. *Annales Geophysicae*, 16(1), 1–24. doi: <https://doi.org/10>
605 [.1007/s00585-997-0001-x](https://doi.org/10.1007/s00585-997-0001-x)
- 606 Burch, J. L., Moore, T. E., Torbert, R. B., & Giles, B. L. (2016). Magnetospheric
607 Multiscale Overview and Science Objectives. *Space Science Reviews*, 199,
608 5–21. doi: <https://doi.org/10.1007/s11214-015-0164-9>
- 609 Burlaga, L. F. (1988). Magnetic clouds and force-free fields with constant alpha.
610 *Journal of Geophysical Research: Space Physics*, 93(A7), 7217–7224. doi:
611 <https://doi.org/10.1029/JA093iA07p07217>
- 612 Chen, Y., Tóth, G., Hietala, H., Vines, S. K., Zou, Y., Nishimura, Y., ... Markidis,
613 S. (2020). Magnetohydrodynamic with embedded particle-in-cell sim-
614 ulation of the geospace environment modeling dayside kinetic processes
615 challenge event. *Earth and Space Science*, 7(11), e2020EA001331. Re-
616 trieved from [https://agupubs.onlinelibrary.wiley.com/doi/abs/](https://agupubs.onlinelibrary.wiley.com/doi/abs/10.1029/2020EA001331)
617 [10.1029/2020EA001331](https://agupubs.onlinelibrary.wiley.com/doi/abs/10.1029/2020EA001331) (e2020EA001331 10.1029/2020EA001331) doi:
618 <https://doi.org/10.1029/2020EA001331>
- 619 Cooling, B. M. A., Owen, C. J., & Schwartz, S. J. (2001). Role of the magne-
620 tosheath flow in determining the motion of open flux tubes. *Journal of*
621 *Geophysical Research: Space Physics*, 106(A9), 18763–18775. Retrieved
622 from [https://agupubs.onlinelibrary.wiley.com/doi/abs/10.1029/](https://agupubs.onlinelibrary.wiley.com/doi/abs/10.1029/2000JA000455)
623 [2000JA000455](https://agupubs.onlinelibrary.wiley.com/doi/abs/10.1029/2000JA000455) doi: <https://doi.org/10.1029/2000JA000455>
- 624 Cowley, S. W. H. (1982). The causes of convection in the earth's magnetosphere:

- 625 A review of developments during the ims. *Reviews of Geophysics*, 20(3), 531-
626 565. Retrieved from [https://agupubs.onlinelibrary.wiley.com/doi/abs/
627 10.1029/RG020i003p00531](https://agupubs.onlinelibrary.wiley.com/doi/abs/10.1029/RG020i003p00531) doi: <https://doi.org/10.1029/RG020i003p00531>
- 628 Dai, L. (2018). Structures of hall fields in asymmetric magnetic reconnection.
629 *Journal of Geophysical Research: Space Physics*, 123, 7332-7341.
630 Retrieved from <http://doi.wiley.com/10.1029/2018JA025251> doi:
631 10.1029/2018JA025251
- 632 Dasso, S., Mandrini, C. H., Démoulin, P., & Farrugia, C. J. (2003). Magnetic
633 helicity analysis of an interplanetary twisted flux tube. *Journal of Geo-
634 physical Research: Space Physics*, 108(A10). Retrieved from [https://
635 agupubs.onlinelibrary.wiley.com/doi/abs/10.1029/2003JA009942](https://agupubs.onlinelibrary.wiley.com/doi/abs/10.1029/2003JA009942) doi:
636 <https://doi.org/10.1029/2003JA009942>
- 637 Denton, R. E., Sonnerup, B. U. ., Hasegawa, H., Phan, T. D., Russell, C. T.,
638 Strangeway, R. J., ... Torbert, R. B. (2016). Reconnection guide field and
639 quadrupolar structure observed by mms on 16 october 2015 at 1307 ut. *Jour-
640 nal of Geophysical Research: Space Physics*, 121(10), 9880-9887. Retrieved
641 from [https://agupubs.onlinelibrary.wiley.com/doi/abs/10.1002/
642 2016JA023323](https://agupubs.onlinelibrary.wiley.com/doi/abs/10.1002/2016JA023323) doi: <https://doi.org/10.1002/2016JA023323>
- 643 Dorelli, J. C., & Bhattacharjee, A. (2009). On the generation and topology of flux
644 transfer events. *Journal of Geophysical Research: Space Physics*, 114(A6).
645 Retrieved from [https://agupubs.onlinelibrary.wiley.com/doi/abs/
646 10.1029/2008JA013410](https://agupubs.onlinelibrary.wiley.com/doi/abs/10.1029/2008JA013410) doi: <https://doi.org/10.1029/2008JA013410>
- 647 Eastwood, J. P., Phan, T. D., Fear, R. C., Sibeck, D. G., Angelopoulos, V., Øieroset,
648 M., & Shay, M. A. (2012). Survival of flux transfer event (fte) flux ropes far
649 along the tail magnetopause. *Journal of Geophysical Research: Space Physics*,
650 117(A8). Retrieved from [https://agupubs.onlinelibrary.wiley.com/doi/
651 abs/10.1029/2012JA017722](https://agupubs.onlinelibrary.wiley.com/doi/abs/10.1029/2012JA017722) doi: <https://doi.org/10.1029/2012JA017722>
- 652 Eastwood, J. P., Phan, T. D., Øieroset, M., Shay, M. A., Malakit, K., Swisdak,
653 M., ... Masters, A. (2013, nov). Influence of asymmetries and guide
654 fields on the magnetic reconnection diffusion region in collisionless space
655 plasmas. *Plasma Physics and Controlled Fusion*, 55(12), 124001. Re-
656 trieved from <https://doi.org/10.1088/0741-3335/55/12/124001> doi:
657 10.1088/0741-3335/55/12/124001

- 658 Escoubet, C. P., Fehringer, M., & Goldstein, M. (2001). Introduction the cluster
659 mission. *Annales Geophysicae*, 19(10/12), 1197-1200. doi: <https://doi.org/10>
660 .5194/angeo-19-1197-2001
- 661 Fargette, N., Lavraud, B., Øieroset, M., Phan, T. D., Toledo-Redondo, S., Kieokaew,
662 R., ... Smith, S. E. (2020). On the ubiquity of magnetic reconnection inside
663 flux transfer event-like structures at the earth's magnetopause. *Geophysical*
664 *Research Letters*, 47(6), e2019GL086726. (e2019GL086726 2019GL086726) doi:
665 <https://doi.org/10.1029/2019GL086726>
- 666 Farrugia, C. J., Chen, L.-J., Torbert, R. B., Southwood, D. J., Cowley, S. W. H.,
667 Vrublevskis, A., ... Smith, C. W. (2011). "crater" flux transfer events: High-
668 road to the x line? *Journal of Geophysical Research: Space Physics*, 116(A2).
669 Retrieved from <https://agupubs.onlinelibrary.wiley.com/doi/abs/>
670 [10.1029/2010JA015495](https://doi.org/10.1029/2010JA015495) doi: <https://doi.org/10.1029/2010JA015495>
- 671 Farrugia, C. J., Rijnbeek, R. P., Saunders, M. A., Southwood, D. J., Rodgers,
672 D. J., Smith, M. F., ... Woolliscroft, L. J. C. (1988). A multi-instrument
673 study of flux transfer event structure. *Journal of Geophysical Research:*
674 *Space Physics*, 93(A12), 14465-14477. Retrieved from <https://agupubs>
675 [.onlinelibrary.wiley.com/doi/abs/10.1029/JA093iA12p14465](https://doi.org/10.1029/JA093iA12p14465) doi:
676 <https://doi.org/10.1029/JA093iA12p14465>
- 677 Fear, R. C., Palmroth, M., & Milan, S. E. (2012). Seasonal and clock an-
678 gle control of the location of flux transfer event signatures at the magne-
679 topause. *Journal of Geophysical Research: Space Physics*, 117(A4). doi:
680 <https://doi.org/10.1029/2011JA017235>
- 681 Guo, J., Lu, S., Lu, Q., Lin, Y., Wang, X., Huang, K., ... Wang, S. (2021). Struc-
682 ture and coalescence of magnetopause flux ropes and their dependence on imf
683 clock angle: Three-dimensional global hybrid simulations. *Journal of Geophysi-*
684 *cal Research: Space Physics*, 126(2), e2020JA028670. Retrieved from <https://>
685 agupubs.onlinelibrary.wiley.com/doi/abs/10.1029/2020JA028670
686 (e2020JA028670 2020JA028670) doi: <https://doi.org/10.1029/2020JA028670>
- 687 Hasegawa, H., Wang, J., Dunlop, M. W., Pu, Z. Y., Zhang, Q. H., Lavraud, B., ...
688 Bogdanova, Y. V. (2010). Evidence for a flux transfer event generated by mul-
689 tiple x-line reconnection at the magnetopause. *Geophysical Research Letters*,
690 37, 1-6. doi: [10.1029/2010GL044219](https://doi.org/10.1029/2010GL044219)

- 691 Hoilijoki, S., Ganse, U., Sibeck, D. G., Cassak, P. A., Turc, L., Battarbee, M., ...
692 Palmroth, M. (2019, jun). Properties of Magnetic Reconnection and FTEs on
693 the Dayside Magnetopause With and Without Positive IMF B x Component
694 During Southward IMF. *Journal of Geophysical Research: Space Physics*,
695 *124*(6), 4037–4048. Retrieved from [https://onlinelibrary.wiley.com/doi/](https://onlinelibrary.wiley.com/doi/abs/10.1029/2019JA026821)
696 [abs/10.1029/2019JA026821](https://onlinelibrary.wiley.com/doi/abs/10.1029/2019JA026821) doi: 10.1029/2019JA026821
- 697 Hwang, K.-J., Nishimura, Y., Coster, A. J., Gillies, R. G., Fear, R. C., Fuselier,
698 S. A., ... Clausen, L. B. (2020). Sequential observations of flux transfer
699 events, poleward-moving auroral forms, and polar cap patches. *Journal of*
700 *Geophysical Research: Space Physics*, *125*(6), e2019JA027674. Retrieved
701 from [https://agupubs.onlinelibrary.wiley.com/doi/abs/10.1029/](https://agupubs.onlinelibrary.wiley.com/doi/abs/10.1029/2019JA027674)
702 [2019JA027674](https://agupubs.onlinelibrary.wiley.com/doi/abs/10.1029/2019JA027674) (e2019JA027674 2019JA027674) doi: [https://doi.org/10.1029/](https://doi.org/10.1029/2019JA027674)
703 [2019JA027674](https://doi.org/10.1029/2019JA027674)
- 704 Karimabadi, H., Krauss-Varban, D., Omid, N., & Vu, H. X. (1999). Magnetic
705 structure of the reconnection layer and core field generation in plasmoids.
706 *Journal of Geophysical Research: Space Physics*, *104*, 12313–12326. doi:
707 [10.1029/1999ja900089](https://doi.org/10.1029/1999ja900089)
- 708 Kieokaew, R., Lavraud, B., Fargette, N., Marchaudon, A., Génot, V., Jacquy, C.,
709 ... Burch, J. (2021). Statistical relationship between interplanetary magnetic
710 field conditions and the helicity sign of flux transfer event flux ropes. *Geophys-*
711 *ical Research Letters*, *48*(6), e2020GL091257. (e2020GL091257 2020GL091257)
712 doi: <https://doi.org/10.1029/2020GL091257>
- 713 King, J. H., & Papitashvili, N. E. (2005). Solar wind spatial scales in and compar-
714 isons of hourly wind and ace plasma and magnetic field data. *Journal of Geo-*
715 *physical Research: Space Physics*, *110*(A2). Retrieved from [https://agupubs](https://agupubs.onlinelibrary.wiley.com/doi/abs/10.1029/2004JA010649)
716 [.onlinelibrary.wiley.com/doi/abs/10.1029/2004JA010649](https://agupubs.onlinelibrary.wiley.com/doi/abs/10.1029/2004JA010649) doi: [https://](https://doi.org/10.1029/2004JA010649)
717 doi.org/10.1029/2004JA010649
- 718 LaBelle, J., Treumann, R. A., Haerendel, G., Bauer, O. H., Paschmann, G., Baumjo-
719 hann, W., ... Holzworth, R. H. (1987). Amplitude observations of waves
720 associated with flux transfer events in the magnetosphere. *Journal of Geophys-*
721 *ical Research: Space Physics*, *92*(A6), 5827–5843. Retrieved from [https://](https://agupubs.onlinelibrary.wiley.com/doi/abs/10.1029/JA092iA06p05827)
722 agupubs.onlinelibrary.wiley.com/doi/abs/10.1029/JA092iA06p05827
723 doi: <https://doi.org/10.1029/JA092iA06p05827>

- 724 Le, A., Egedal, J., Daughton, W., Fox, W., & Katz, N. (2009, Feb). Equa-
 725 tions of state for collisionless guide-field reconnection. *Phys. Rev. Lett.*,
 726 *102*, 085001. Retrieved from [https://link.aps.org/doi/10.1103/](https://link.aps.org/doi/10.1103/PhysRevLett.102.085001)
 727 [PhysRevLett.102.085001](https://link.aps.org/doi/10.1103/PhysRevLett.102.085001) doi: 10.1103/PhysRevLett.102.085001
- 728 Leamon, R. J., Canfield, R. C., Jones, S. L., Lambkin, K., Lundberg, B. J., &
 729 Pevtsov, A. A. (2004). Helicity of magnetic clouds and their associated
 730 active regions. *Journal of Geophysical Research: Space Physics*, *109*(A5).
 731 Retrieved from [https://agupubs.onlinelibrary.wiley.com/doi/abs/](https://agupubs.onlinelibrary.wiley.com/doi/abs/10.1029/2003JA010324)
 732 [10.1029/2003JA010324](https://doi.org/10.1029/2003JA010324) doi: <https://doi.org/10.1029/2003JA010324>
- 733 Lee, L. C., & Fu, Z. F. (1985). A theory of magnetic flux transfer at the earth's
 734 magnetopause. *Geophysical Research Letters*, *12*(2), 105-108. doi: [https://doi](https://doi.org/10.1029/GL012i002p00105)
 735 [.org/10.1029/GL012i002p00105](https://doi.org/10.1029/GL012i002p00105)
- 736 Lepping, R. P., Jones, J. A., & Burlaga, L. F. (1990). Magnetic field structure of
 737 interplanetary magnetic clouds at 1 au. *Journal of Geophysical Research*, *95*,
 738 11957. doi: 10.1029/ja095ia08p11957
- 739 Lundquist, S. (1950). Magnetohydrostatic fields. *Arkiv För Fyzik*, *2*(35), 361-365.
- 740 Mandt, M. E., Denton, R. E., & Drake, J. F. (1994). Transition to whistler me-
 741 diated magnetic reconnection. *Geophysical Research Letters*, *21*(1), 73-76.
 742 Retrieved from [https://agupubs.onlinelibrary.wiley.com/doi/abs/](https://agupubs.onlinelibrary.wiley.com/doi/abs/10.1029/93GL03382)
 743 [10.1029/93GL03382](https://doi.org/10.1029/93GL03382) doi: <https://doi.org/10.1029/93GL03382>
- 744 Martin, C. J., Arridge, C. S., Badman, S. V., Billett, D. D., & Barratt, C. J.
 745 (2020). Modeling non-force-free and deformed flux ropes in titan's ionosphere.
 746 *Journal of Geophysical Research: Space Physics*, *125*(4), e2019JA027571.
 747 Retrieved from [https://agupubs.onlinelibrary.wiley.com/doi/abs/](https://agupubs.onlinelibrary.wiley.com/doi/abs/10.1029/2019JA027571)
 748 [10.1029/2019JA027571](https://doi.org/10.1029/2019JA027571) (e2019JA027571 10.1029/2019JA027571) doi:
 749 <https://doi.org/10.1029/2019JA027571>
- 750 Mozer, F. S., & Hull, A. (2010). Scaling the energy conversion rate from magnetic
 751 field reconnection to different bodies. *Physics of Plasmas*, *17*(10), 102906. Re-
 752 trieved from <https://doi.org/10.1063/1.3504224> doi: 10.1063/1.3504224
- 753 Nagai, T., Shinohara, I., Fujimoto, M., Hoshino, M., Saito, Y., Machida, S., &
 754 Mukai, T. (2001). Geotail observations of the hall current system: Evi-
 755 dence of magnetic reconnection in the magnetotail. *Journal of Geophysical*
 756 *Research: Space Physics*, *106*(A11), 25929-25949. Retrieved from <https://>

- 757 agupubs.onlinelibrary.wiley.com/doi/abs/10.1029/2001JA900038 doi:
758 <https://doi.org/10.1029/2001JA900038>
- 759 Øieroset, M., Phan, T. D., Eastwood, J. P., Fujimoto, M., Daughton, W., Shay,
760 M. A., ... Glassmeier, K.-H. (2011, Oct). Direct evidence for a three-
761 dimensional magnetic flux rope flanked by two active magnetic reconnection
762 x lines at earth's magnetopause. *Phys. Rev. Lett.*, *107*, 165007. Retrieved
763 from <https://link.aps.org/doi/10.1103/PhysRevLett.107.165007> doi:
764 10.1103/PhysRevLett.107.165007
- 765 Pal, S. (2022). Uncovering the process that transports magnetic helicity to coro-
766 nal mass ejection flux ropes. *Advances in Space Research*, *70*(6), 1601-1613.
767 Retrieved from [https://www.sciencedirect.com/science/article/pii/](https://www.sciencedirect.com/science/article/pii/S0273117721008620)
768 [S0273117721008620](https://www.sciencedirect.com/science/article/pii/S0273117721008620) (Magnetic Flux Ropes in Solar Environments) doi:
769 <https://doi.org/10.1016/j.asr.2021.11.013>
- 770 Paschmann, G., Haerendel, G., Papamastorakis, I., Sckopke, N., Bame, S. J.,
771 Gosling, J. T., & Russell, C. T. (1982). Plasma and magnetic field character-
772 istics of magnetic flux transfer events. *Journal of Geophysical Research: Space*
773 *Physics*, *87*(A4), 2159-2168. doi: <https://doi.org/10.1029/JA087iA04p02159>
- 774 Pollock, C., Moore, T., Jacques, A., Burch, J., Gliese, U., Saito, Y., ... Zeuch, M.
775 (2016). Fast Plasma Investigation for Magnetospheric Multiscale. *Space Sci-*
776 *ence Reviews*, *199*, 331-406. doi: <https://doi.org/10.1007/s11214-016-0245-4>
- 777 Raeder, J. (2006). Flux transfer events: 1. generation mechanism for strong south-
778 ward imf. *Annales Geophysicae*, *24*(1), 381-392. doi: [https://doi.org/10.5194/](https://doi.org/10.5194/angeo-24-381-2006)
779 [angeo-24-381-2006](https://doi.org/10.5194/angeo-24-381-2006)
- 780 Rijnbeek, R. P., Cowley, S. W. H., Southwood, D. J., & Russell, C. T. (1982).
781 Observations of reverse polarity flux transfer events at the earth's dayside
782 magnetopause. *Nature*, *300*, 23-26. doi: <https://doi.org/10.1038/300023a0>
- 783 Russell, C. T. (1990). Magnetic flux ropes in the ionosphere of venus. In *Physics*
784 *of magnetic flux ropes* (p. 413-423). American Geophysical Union (AGU).
785 Retrieved from [https://agupubs.onlinelibrary.wiley.com/doi/abs/](https://agupubs.onlinelibrary.wiley.com/doi/abs/10.1029/GM058p0413)
786 [10.1029/GM058p0413](https://agupubs.onlinelibrary.wiley.com/doi/abs/10.1029/GM058p0413) doi: <https://doi.org/10.1029/GM058p0413>
- 787 Russell, C. T., Anderson, B. J., Baumjohann, W., Bromund, K. R., Dearborn, D.,
788 Fischer, D., ... Richter, I. (2016). The Magnetospheric Multiscale Magne-
789 tometers. *Space Science Reviews*, *199*, 189-256. doi: <https://doi.org/10.1007/>

790
791
792
793
794
795
796
797
798
799
800
801
802
803
804
805
806
807
808
809
810
811
812
813
814
815
816
817
818
819
820
821
822

- s11214-014-0057-3
- Russell, C. T., & Elphic, R. C. (1978). Initial isee magnetometer results: magnetopause observations. *Space Science Review*, *22*, 681–715. doi: <https://doi.org/10.1007/BF00212619>
- Russell, C. T., & Elphic, R. C. (1979). Isee observations of flux transfer events at the dayside magnetopause. *Geophysical Research Letters*, *6*(1), 33-36. doi: <https://doi.org/10.1029/GL006i001p00033>
- Rème, H., Bosqued, J. M., Sauvaud, J. A., Cros, A., Dandouras, J., Aoustin, C., ... Chionchio, G. (1997). The Cluster Ion Spectrometry Experiment. *Space Science Reviews*, *78*, 303–350. doi: <https://doi.org/10.1023/A:1004929816409>
- Saunders, M. A., Russell, C. T., & Sckopke, N. (1984). Flux transfer events: Scale size and interior structure. *Geophysical Research Letters*, *11*(2), 131-134. Retrieved from <https://agupubs.onlinelibrary.wiley.com/doi/abs/10.1029/GL011i002p00131> doi: <https://doi.org/10.1029/GL011i002p00131>
- Scholer, M. (1988). Magnetic flux transfer at the magnetopause based on single x line bursty reconnection. *Geophysical Research Letters*, *15*(4), 291-294. Retrieved from <https://agupubs.onlinelibrary.wiley.com/doi/abs/10.1029/GL015i004p00291> doi: <https://doi.org/10.1029/GL015i004p00291>
- Shue, J.-H., Song, P., Russell, C. T., Steinberg, J. T., Chao, J. K., Zastenker, G., ... Kawano, H. (1998). Magnetopause location under extreme solar wind conditions. *Journal of Geophysical Research: Space Physics*, *103*(A8), 17691-17700. doi: <https://doi.org/10.1029/98JA01103>
- Sibeck, D. G., Kuznetsova, M., Angelopoulos, V., Glaßmeier, K.-H., & McFadden, J. P. (2008). Crater ftes: Simulation results and themis observations. *Geophysical Research Letters*, *35*(17). Retrieved from <https://agupubs.onlinelibrary.wiley.com/doi/abs/10.1029/2008GL033568> doi: <https://doi.org/10.1029/2008GL033568>
- Song, Y., & Lysak, R. L. (1989). Evaluation of twist helicity of flux transfer event flux tubes. *Journal of Geophysical Research: Space Physics*, *94*(A5), 5273-5281. Retrieved from <https://agupubs.onlinelibrary.wiley.com/doi/abs/10.1029/JA094iA05p05273> doi: <https://doi.org/10.1029/JA094iA05p05273>
- Southwood, D., Farrugia, C., & Saunders, M. (1988). What are flux transfer events? *Planetary and Space Science*, *36*(5), 503-508. Retrieved from

- 823 <https://www.sciencedirect.com/science/article/pii/0032063388901092>
824 doi: [https://doi.org/10.1016/0032-0633\(88\)90109-2](https://doi.org/10.1016/0032-0633(88)90109-2)
- 825 Teh, W. L., Abdullah, M., & Hasbi, A. M. (2014). Evidence for the core
826 field polarity of magnetic flux ropes against the reconnection guide field.
827 *Journal of Geophysical Research: Space Physics*, *119*, 8979-8983. doi:
828 10.1002/2014JA020509
- 829 Teh, W.-L., Nakamura, R., Karimabadi, H., Baumjohann, W., & Zhang, T. L.
830 (2014). Correlation of core field polarity of magnetotail flux ropes with
831 the imf by: Reconnection guide field dependency. *Journal of Geophysi-*
832 *cal Research: Space Physics*, *119*(4), 2933-2944. Retrieved from [https://](https://agupubs.onlinelibrary.wiley.com/doi/abs/10.1002/2013JA019454)
833 agupubs.onlinelibrary.wiley.com/doi/abs/10.1002/2013JA019454 doi:
834 <https://doi.org/10.1002/2013JA019454>
- 835 Trattner, K. J., Mulcock, J. S., Petrinec, S. M., & Fuselier, S. A. (2007). Location
836 of the reconnection line at the magnetopause during southward imf condi-
837 tions. *Geophysical Research Letters*, *34*(3). doi: [https://doi.org/10.1029/](https://doi.org/10.1029/2006GL028397)
838 [2006GL028397](https://doi.org/10.1029/2006GL028397)
- 839 Trenchi, L., Coxon, J. C., Fear, R. C., Eastwood, J. P., Dunlop, M. W., Trattner,
840 K. J., ... Lavraud, B. (2019). Signatures of magnetic separatrices at the
841 borders of a crater flux transfer event connected to an active x-line. *Jour-*
842 *nal of Geophysical Research: Space Physics*, *124*(11), 8600-8616. Retrieved
843 from [https://agupubs.onlinelibrary.wiley.com/doi/abs/10.1029/](https://agupubs.onlinelibrary.wiley.com/doi/abs/10.1029/2018JA026126)
844 [2018JA026126](https://agupubs.onlinelibrary.wiley.com/doi/abs/10.1029/2018JA026126) doi: <https://doi.org/10.1029/2018JA026126>
- 845 Trenchi, L., Marcucci, M. F., Rème, H., Carr, C. M., & Cao, J. B. (2011). Tc-1 ob-
846 servations of a flux rope: Generation by multiple x line reconnection. *Journal*
847 *of Geophysical Research: Space Physics*, *116*(A5). Retrieved from [https://](https://agupubs.onlinelibrary.wiley.com/doi/abs/10.1029/2010JA015986)
848 agupubs.onlinelibrary.wiley.com/doi/abs/10.1029/2010JA015986 doi:
849 <https://doi.org/10.1029/2010JA015986>
- 850 Wei, H., Russell, C., Zhang, T., & Dougherty, M. (2010). Comparison study of
851 magnetic flux ropes in the ionospheres of venus, mars and titan. *Icarus*,
852 *206*(1), 174-181. Retrieved from [https://www.sciencedirect.com/science/](https://www.sciencedirect.com/science/article/pii/S001910350900116X)
853 [article/pii/S001910350900116X](https://www.sciencedirect.com/science/article/pii/S001910350900116X) (Solar Wind Interactions with Mars) doi:
854 <https://doi.org/10.1016/j.icarus.2009.03.014>
- 855 Wright, A. N., & Berger, M. A. (1990). The interior structure of recon-

- 856 nected flux tubes in a sheared plasma flow. *Journal of Geophysical Re-*
857 *search: Space Physics*, 95(A6), 8029-8036. Retrieved from [https://](https://agupubs.onlinelibrary.wiley.com/doi/abs/10.1029/JA095iA06p08029)
858 agupubs.onlinelibrary.wiley.com/doi/abs/10.1029/JA095iA06p08029
859 doi: <https://doi.org/10.1029/JA095iA06p08029>
- 860 Zhang, H., Kivelson, M. G., Angelopoulos, V., Khurana, K. K., Pu, Z. Y., Walker,
861 R. J., ... Phan, T. (2012). Generation and properties of in vivo flux transfer
862 events. *Journal of Geophysical Research: Space Physics*, 117(A5). Retrieved
863 from [https://agupubs.onlinelibrary.wiley.com/doi/abs/10.1029/](https://agupubs.onlinelibrary.wiley.com/doi/abs/10.1029/2011JA017166)
864 [2011JA017166](https://agupubs.onlinelibrary.wiley.com/doi/abs/10.1029/2011JA017166) doi: <https://doi.org/10.1029/2011JA017166>
- 865 Zhang, H., Kivelson, M. G., Khurana, K. K., McFadden, J., Walker, R. J., An-
866 gelopoulos, V., ... Auster, H. U. (2010). Evidence that crater flux trans-
867 fer events are initial stages of typical flux transfer events. *Journal of Geo-*
868 *physical Research: Space Physics*, 115(A8). Retrieved from [https://](https://agupubs.onlinelibrary.wiley.com/doi/abs/10.1029/2009JA015013)
869 agupubs.onlinelibrary.wiley.com/doi/abs/10.1029/2009JA015013 doi:
870 <https://doi.org/10.1029/2009JA015013>
- 871 Zhang, Y. C., Lavraud, B., Dai, L., Wang, C., Marchaudon, A., Avanov, L.,
872 ... Torbert, R. (2017). Quantitative analysis of a hall system in the
873 exhaust of asymmetric magnetic reconnection. *Journal of Geophysical*
874 *Research: Space Physics*, 122(5), 5277-5289. Retrieved from [https://](https://agupubs.onlinelibrary.wiley.com/doi/abs/10.1002/2016JA023620)
875 agupubs.onlinelibrary.wiley.com/doi/abs/10.1002/2016JA023620 doi:
876 <https://doi.org/10.1002/2016JA023620>